Uncovering Transport Properties of 4,4′-Bipyridine/Gold Molecular Nanobridges

Ángel J. Pérez-Jiménez*

Departamento de Química-Física, Universidad de Alicante, E-03080 Alicante, Spain

Received: December 10, 2004; In Final Form: February 28, 2005

Here, the fascinating connection between the chemical and the transport properties of recently fabricated 4,4′-bipyridine/gold nanobridges (Xu, B.; Tao, N. J. *Science* **2003**, *301*, 1221) is addressed. By means of first-principles ab initio calculations, the remarkable reproducibility of the 4,4′-bipyridine conductance properties is explained as the combined result of (i) the bonding of the molecule to the metallic leads through hybridization between the 4,4′-bipyridine highest occupied molecular orbitals and lowest unoccupied molecular orbitals (LUMOs) with s and d orbitals at low-coordination gold atoms, (ii) the limited number of molecule−lead arrangements due to gold−hydrogen steric repulsions, and (iii) the electron transmission through a LUMO-derived resonance, whose positioning with respect to the Fermi level determines which of the above arrangements yields nonnegligible conductance. Structural and electronic interpretations to the stepped dependence reported for the electronic transport of 4,4′-bipyridine as a function of the distance between the gold tips are also given.

1. Introduction

Researchers worldwide have always sought fruitful combinations of solids and molecules. A new driving force for this effort emerged when it became possible to integrate a few molecules as the key part of electronic circuits. Molecular nanobridges (MNBs) can be built from metallic nanoconstrictions[1−7] by attaching just a few or even a single molecule within the metal electrodes, which opens up an unprecedented number of possibilities in molecular nanoelectronic technologies under development today.[8−15] However, it is still hard to have fine control over such "nanodevices", and a careful analysis of the events occurring during the fabrication process of MNBs is mandatory if one wants to understand, modify, and improve their appealing properties. This is a challenging problem that requires knowledge not only of the processes affecting the formation of the metallic nanocontact but also of the chemical characteristics of the molecule−metal interaction and how these phenomena cooperate to explain the properties of the device. Unfortunately, the experimental conditions are such that it is not always possible to appropriately acquire this information from the measurements alone. There exists a large variability in the structural details of the atoms in the contact, which may change from experiment to experiment, and meaningful information can often be gathered only after performing a statistical analysis over hundreds or even thousands of experiments.[7] However, whenever there is some preferred configuration, a distinguishable pattern is revealed in the corresponding histograms.[15] At that point, the theoretical evaluation of electronic transport helps in the interpretation of the experiments by proposing a set of atomistic configurations compatible with the measurements.[16]

The vast majority of MNBs studied so far have been done in such a way that the molecule "anchoring" to the metal nanocontact comes from the gas phase. However, recent work by Tao and co-workers has focused on studying nanostructures in liquid solutions at room temperature.[17,18] Especially remarkable is a recent experiment by Xu and Tao,[19] where they measure the conducting properties of a MNB where a gold nanocontact using a scanning tunneling microscope (STM) is formed in an aqueous $NaClO_4$ solution of 4,4′-bipyridine (44bpy). Apart from the usual quantization of the conductance observed in the process of breaking the gold nanocontact, additional quantization features appear that the authors associate with the 44bpy molecule. In particular, Xu and Tao report conductance plateaus of $0.01G_0$, $0.02G_0$, and $0.03G_0$ in conductance versus STM displacement traces just after the breaking of the gold nanocontact has taken place. ($G_0 = 2e^2/h$ is the so-called conductance quantum.) The fact that these plateaus disappear when the 44bpy molecules are removed from the solution and also that their size is about that of the 44bpy molecule led the authors to conclude that this phenomenon was due to the formation of conducting 44bpy/gold nanobridges. The extraordinary reproducibility of these conductance plateaus, confirmed by the narrow peaks found in the corresponding conductance histograms over 1000 experiments, is certainly one of the most outstanding results from this experiment. Clarification of the phenomena leading to this enhanced reproducibility would help scientists in this field to design better MNBs. Furthermore, the authors ascribe the $1 \times G_0$, $2 \times G_0$, and $3 \times G_0$ plateaus to one, two, and three molecules, respectively, forming the nanobridge. This is supported by the stepped shape found in some traces, where the plateaus, in decreasing order of magnitude, appear sequentially one after the other upon elongation of the metallic contacts.

The main purpose of this paper is to elucidate the relationship between the physicochemical and transport properties of 44bpy/gold nanobridges, by answering the following questions, which arise from the above-mentioned experimental findings:

1. Is the remarkable reproducibility of the 44bpy/gold conductance plateaus related with some preferred configurations of the atoms in this MNB?

2. If so, what are the chemical reasons for such a preference?

3. What is the role played by the electronic structure of 44bpy in the conductance properties of this MNB?

* Author to whom correspondence should be addressed. E-mail: aj.perez@ua.es.

10.1021/jp044370b CCC: $30.25
Published on Web 04/23/2005

4. What is the mechanism that leads to such large plateaus and their, sometimes, stepped behavior?

In the following sections, strong theoretical evidence will be given to support the claim that the answer to question 1 is affirmative, mainly due to the presence of steric repulsions between the gold atoms in the metallic tips and the foremost hydrogens in the heterocycles of the 44bpy molecule. This limits the ways that the molecule attaches to the metallic background to some preferred configurations. As for question 3, it will be seen that the subsequent alignment of the molecular energy levels with respect to the Fermi energy of the overall system (by means of a charge transfer process) is different for each of this small set of configurations. Additionally, conduction through the MNB is controlled by a resonance developed from the 44bpy lowest unoccupied molecular level (LUMO), with only one of the above configurations placing this resonance with respect to the Fermi level in such a way so as to give a conductance compatible with the experimental result. It will also be found that this geometry provides an explanation to question 4, bringing internal consistency to the theoretical description of the events taking place in the experiments reported in ref 19.

The interdisciplinary character of the subject makes it worthwhile to introduce some crucial concepts related with the calculations presented in this work, which is done in the next section. In section 3, the structure of the gold nanocontact alone is studied, to reduce as much as possible the number of relevant structures that provide a suitable place for anchoring the 44bpy molecules. Section 4 then presents and discusses the main results of this work, sketched in the previous paragraph, stressing the relationship between the chemical and transport properties of this type of MNB. Finally, the last section is devoted to summarize all this information and to extract some clues that may help to design MNBs with *reproducible* and well-known conductance properties *despite* the varying geometries that the underlying metal nanocontact may adopt.

2. Formalism and Computations

The problem of theoretically determining the conductance of a nanodevice is a rather involved one and requires some expertise on both solid-state physics and molecular chemistry. Notwithstanding these, electronic transport through nanodevices stems from just two simple facts:

1. At the atomic scale, particles show wavelike properties.

2. Transport can be measured in a wavelike picture as how much of each incident wave (electron wave function) is transmitted throughout the region of interest.

These two basic premises have been worked through by a number of researchers (see, e.g., ref. 7) and can be summarized into an expression for the conductance of a nanodevice valid under some restrictions usually met in the experiments. The zero-temperature limit of this expression, also known as Landauer's formula, may adopt a friendly look

$$G(E_F) = \frac{2e^2}{h} \sum_i T_i(E_F) \qquad (1)$$

(with e, h, and E_F being, respectively, the electron charge, Planck's constant, and the Fermi energy) or a not so simple one

$$G(E_F) = \frac{2e^2}{h} \mathrm{Tr}[\mathbf{\Gamma}_L(E_F)\mathbf{G}^r(E_F)\mathbf{\Gamma}_R(E_F)\mathbf{G}^a(E_F)] \qquad (2)$$

Both equations yield the same result, although the first one more explicitly shows that the conductance originates from the contribution of electrons traversing the MNB through several *channels* (built up from the coupling of the molecular and electrode wave functions) each one having a definite value for the *transmission* T_i (see point 2 above).

However, eq 2 may seem an arcane one at first sight, but it only reflects the fact that to compute the conductance the system can be divided into two parts, a finite region containing the molecule and two semi-infinite regions including the rest of each electrode. Within this scheme, the conductance depends both on the coupling between the finite region and the rest of the left and right electrodes, represented by the matrixes $\mathbf{\Gamma}_L$ and $\mathbf{\Gamma}_R$, and on the electronic structure of that finite region, embedded in the so-called *retarded*, $\mathbf{G}^r$, and *advanced*, $\mathbf{G}^a$, Green's functions, which can be obtained from Dyson's equation[20]

$$[(E \pm i\delta)\mathbf{I} - \mathbf{H} - \Sigma^{r(a)}(E)]\mathbf{G}^{r(a)}(E) = \mathbf{I} \qquad (3)$$

where $\mathbf{I}$ and δ represent the identity matrix and an infinitesimal positive number, respectively. To solve this equation, one needs the Hamiltonian matrix of the finite region $\mathbf{H}$ and the so-called self-energy matrices $\mathbf{\Sigma}^{r(a)}$ representing the perturbation caused to that region when connecting it to the semi-infinite electrodes. The coupling matrixes $\mathbf{\Gamma}_{L(R)}$ are obtained from the latter as

$$\mathbf{\Gamma}_{L(R)} = i(\mathbf{\Sigma}^r_{L(R)} - \mathbf{\Sigma}^a_{L(R)}) \qquad (4)$$

As denoted above, both the Green's functions and the self-energies are energy-dependent, but the important quantity is their value *at* the energy of the conducting electrons, or Fermi energy, which is not known a priori. The basic caveats to solve eq 3 are:

(i) The methodology selected to calculate $\mathbf{H}$.

(ii) The model used to approximate $\mathbf{\Sigma}^{r(a)}$.

(iii) The procedure followed to obtain the Fermi energy.

Several approaches can be found in the literature implementing the above equations that differ in the way they solve points i−iii.[21−31] Throughout this work, the so-called *Gaussian embedded cluster method* (GECM),[29,31,32] which has proven to be an accurate procedure to calculate transport properties in a number of nanodevices, including metallic nanoconstrictions[31,32] and MNBs involving fullerenes,[29,33] nanotubes,[34] or hydrogen molecules, will be used.[16] Although the interested reader can find a deep description of the method in the above papers, note that GECM uses density functional theory (DFT) to tackle point i and that an efficient recursive Bethe lattice tight-binding model is used as the approach in point ii. In regards to point iii, the method guarantees a common electrochemical potential throughout the entire system (composed of the semi-infinite electrodes and the finite region containing the molecule and a significant part of the leads). This is accomplished by imposing overall charge neutrality in the finite region to find out its electrochemical potential and aligning the electrochemical potential of the electrodes to the latter. Finally, a procedure is used to force overall self-consistency; the density matrix obtained from the Green's function is used to reevaluate the Hamiltonian $\mathbf{H}$, which, in turn, is used to obtain a new estimate of $\mathbf{G}^{r(a)}$ via eq 3; this cycle is repeated until the change in the density matrix is appropriately small.

Apart from points i−iii above, any theoretical approach aimed at *quantitatively predicting* the conductance properties of a MNB should also take into account the relative positions of the atoms in the nanoconstriction. For this reason, geometry optimizations

of small clusters representing the finite part of the nanodevice are made before "connecting" them to semi-infinite electrodes to evaluate the conductance. The optimizations have been done using also DFT and the Gaussian03 package,[35] with the same combination of exchange-correlation functional, basis set, and pseudopotentials used for the conductance calculations (from now on such a combination is referred to as "model chemistry"). More precisely, the hybrid B3LYP exchange-correlation functional[35−37] has been used in combination with the pseudopotential and minimum basis set proposed by Christiansen and co-workers in refs 38 and 39 with contractions Au[3s3p4d]/[1s1p1d], C[4s4p]/[1s1p] and N[4s4p]/[1s1p], while a STO-3G basis has been chosen for the hydrogen atoms. Despite the small size of the basis set, this model chemistry has reasonably described charge transfer, binding energies, and optimized geometries between gold surfaces and fullerenes,[33] providing conductance values consistent with experimental data in metallic Pt−Pt,[16] Au−Au,[31] and Al−Al[31] nanocontacts as well as in fullerene[33] or nanotube[34] molecular nanobridges. In ref 16, H−Pt nanobridges were also studied. However, the small size of the hydrogen molecule allowed the use of a larger basis set[40] on the hydrogen atom to perform the conductance calculations and the vibrational analysis needed for comparison with the experimental results.[15] The validity of the geometries obtained in this work with this limited basis set has also been checked by comparing the results achieved with the much larger LANL2DZ[41−44] basis set and pseudopotential.

However, note that the geometry optimizations performed in this work do not include all the degrees of freedom of the corresponding clusters. In regards to the 44bpy molecule, only its dihedral angle has been allowed to vary in the optimizations. The rest of the 44bpy internal degrees of freedom have been kept frozen to those determined experimentally in the gas phase,[45] because it has been checked that their influence in the results is negligible, while its inclusion would largely increase the computational load. Additional restrictions are posed on the gold coordinates in the optimizations to appropriately represent the experiments, which will be clearly indicated in the text and further documented in the Supporting Information.

3. Gold Nanocontact Breakage

Before directly attempting the calculation of the conductance properties in 44bpy/gold MNBs, the problem of the underlying gold nanocontact alone is first studied. This detour is taken because the MNB forms upon *rupture* of the metallic nanocontact. Hence, it is necessary to elucidate the positions of the metal atoms during the last stages of this rupture, prior to the study of the molecule−metal interaction. This goal will be achieved by a mixed approach, combining the knowledge present in the vast literature on metallic nanocontacts with theoretical calculations. In this manner, at the end of this section, a small set of structures representing the metallic part of this MNB will be proposed.

3.1. About Tips. One of the most striking features observed in metallic nanocontacts is the quantization of the conductance, with *plateaus* appearing at integer multiples of the conductance quantum, G_0, in conductance versus elongation curves. There is now a widespread consensus that this stepped behavior in the number of transmission channels (at least for gold) comes from abrupt plastic deformations only a few atoms in thickness in a nanocontact already only a few atoms in width, followed by elastic phases where no sudden atomic rearrangements take place.[7] Indeed, the strong relationship between conductance quantization and nanocontact structure explains the latter being subject of much interest during the past decade. Thanks to this effort, it has become clear that the structure of gold nanocontacts is crystalline.[5,46−48] Furthermore, it has been pointed out that, when the elongation axis coincides with either the [111] or the [001] crystallographic directions of the face-centered-cubic structure typical of gold, there is a natural tendency to form stable tips,[46,49] while thick wires several atoms wide have been reported for the [011] direction.[46,49,50] Nevertheless, elongation through the [011] direction can also lead to atomic chains,[3,6] which have been associated with extremely large conductance plateaus.[3,4,6,51−53]

The above findings allow the reduction of the number of metallic arrangements that need to be examined. This number can be reduced a bit further if it is taken into account that (a) the last conductance plateaus of the gold nanocontacts reported in Tao's works are about 2 Å wide[17,19] and (b) the bipyridine-related conductance plateaus found by Xu and Tao are observed *after* the last conductance plateau of one quantum unit typical of gold.[19] Therefore, gold nanocontacts leading to short plateaus of one conductance quantum have to be considered. This makes it reasonable to discard (011) structures at the outset since they yield either long atomic chains with *large* $1G_0$ conductance plateaus or stable gold wires with conductances well *above* $1G_0$.

3.2. Quest for the Conductance Quantum. From the discussion in the last section and also from previous theoretical evaluations of the conductance on a number of gold structures,[31,49,54] this study has been directed toward the following gold geometries representing the narrowest part of the nanocontact

(001)	stack fault	9-4-1-1-4-9	Figure 1a
	correct stack	9-4-1-4-9	Figure 1c
(111)	stack fault	6-3-1-1-3-6	Figure 1b
		6-3-1-3-6	Figure 1d
	correct stack	9-5-2-1-3-6	Figure 2

The different structures have been classified according to three parameters, namely, (a) the direction of the longitudinal axis, (b) the preservation of the stacking in the bulk along this axis, and (c) the number of atoms that are present in each plane perpendicular to the longitudinal axis. The scheme above refers to the pertinent figures depicting each geometry. The first four structures are usually considered in theoretical calculations regarding the conductance of gold nanocontacts,[31,49,54] while the last one has not received much attention, yet it will be of major importance to explain a number of experimental findings on gold nanocontacts and 44bpy/gold MNBs, as will be shown below.

Figures 1a−1d and Figure 2 collect both the optimized geometries and their conductance profiles after applying GECM, corresponding to the structures mentioned above. The coordinates of the gold atoms in the outermost planes have been kept frozen to their bulk values in these optimizations to consider the effect of the remaining gold atoms in each electrode, which, although absent in the calculations, impose a certain positioning on the outermost layer of the cluster atoms. The coordinates of the remaining atoms are left completely free to vary in the optimizations. It has also been checked that relaxation of the nanoconstriction width has a minor influence on the conductance. This has been done for the test case of the 9-4-1-1-4-9 structure by including in the optimization the coordinates along the tip−tip axis of the gold atoms in the outermost planes. The corresponding conductance profile is also shown in Figure 1a.

After inspection of Figures 1 and 2, it is evident that the (111) 9-5-2-1-3-6 geometry is a good candidate to represent the rupture of the gold nanocontact. This structure yields a conductance

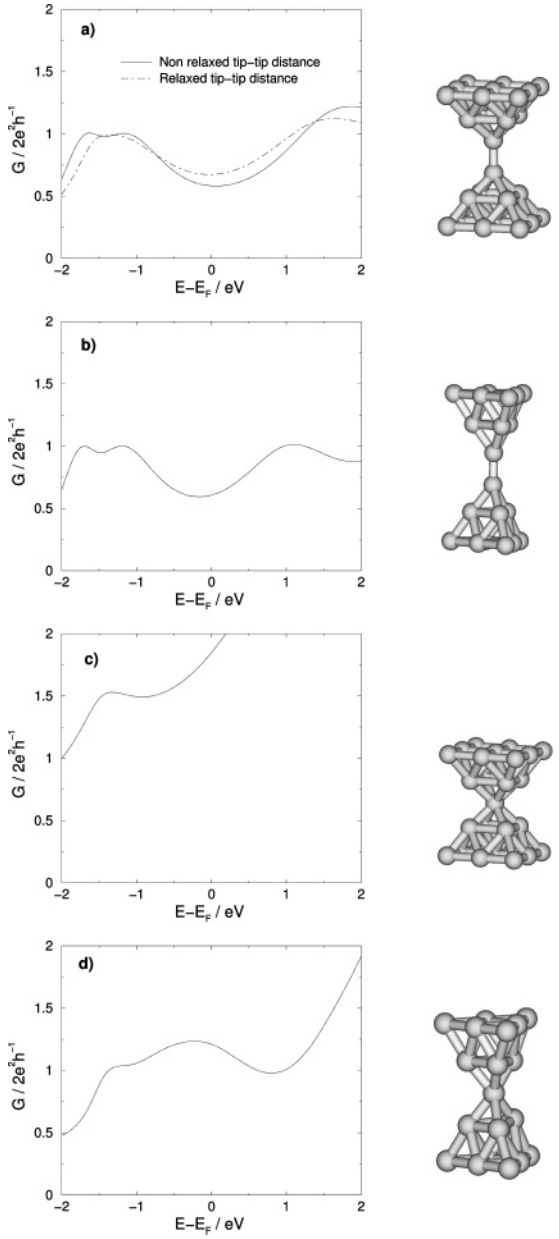

Figure 1. Conductance profiles for the gold nanocontacts depicted at the right: (a) (001) 9-4-1-1-4-9, (b) (111) 6-3-1-1-3-6, (c) (001) 9-4-1-4-9, (d) (111) 6-3-1-3-6. The digits represent the number of atoms in each plane perpendicular to the longitudinal axis.

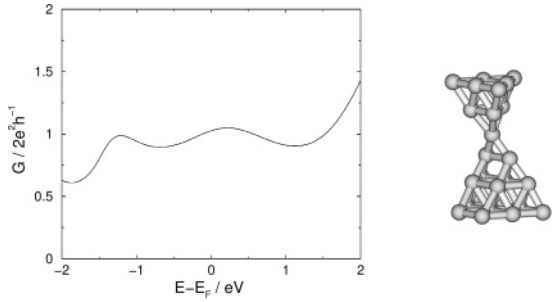

Figure 2. Conductance profile for the (111) 9-5-2-1-3-6 gold nanocontact.

profile with an ample region around the Fermi level where the conductance has minor deviations from $1G_0$. Indeed, it will be seen in the next sections that this type of structure is key to explain additional experimental findings regarding the 44bpy/gold MNBs. However, MNBs resulting from (001) 9-4-1-1-4-9, (111) 6-3-1-1-3-6, and (111) 6-3-1-3-6 gold nanocontact geometries will also be included in the analysis, because they provide conductance values around $1G_0$ and also because of the variety of atomic arrangements that are to be expected from the kind of statistical study performed in ref 19. However, the (001) 9-4-1-4-9 structure will be discarded due to its marked deviation from $1G_0$.

4. Conductance of 44bpy/Gold MNBs

Once the number of possible structures of the underlying metal substrate have been reduced, it is now time to address the main objective of this paper, namely, to find out the connection between the physicochemical and the transport properties of 44bpy/gold MNBs. To fulfill this task, the following need to be known:

1. The geometries of the MNBs that form between 44bpy molecules and the gold tips.

2. The electronic details of the metal−molecule interaction and its influence on the transport properties of this type of MNB. For this, which orbitals contribute to the electronic transport channels as well as their relative positioning with respect to the Fermi energy of the whole system (molecule + electrodes) need to be known.

3. The dependence of the 44bpy/gold nanobridge conductance with respect to the metallic tip−tip distance to explain the size of the conductance plateaus observed in the experiments.

While the vast accumulation of knowledge regarding gold nanocontacts helped to reduce the number of metallic structures that are relevant to this MNB, no such simplification is feasible when it comes to molecule−metallic tip binding. Therefore, points 1−3 above will be tackled solely by means of ab initio calculations. Items 1 and 2 are undertaken first in the next section, where the results will lead to the conclusion that only one type of MNB geometry out of the set of structures analyzed yields a conductance compatible with the experimental result, which explains the marked reproducibility for the conductance of 44bpy/gold MNBs. This geometry will be used in a subsequent section that will address point 3 above. Given the variability in the experimental measurements performed in ref 19, it is clear that several structures can contribute to each peak in the histograms. Therefore, the structure that is proposed here should be regarded as the representative of a family of similar atomic arrangements that contributes most to the peak maximum.

Before continuing, note the absence of the solvent and the solute in the calculations that have been performed. Although this may have some effect on the results achieved in this work, the experimental evidence suggests that it would be of minor importance. First of all, according to Tao et al.,[18] neither Na^+ nor ClO_4^- tend to adsorb at the gold surface, and hence they do not act as dopants. Second, the conductance quantization of gold nanocontacts is unaltered in $NaClO_4$ solutions at positive potentials with respect to a reference electrode.[17] Thus, water molecules and the surrounding Na^+ and ClO_4^- ions do not alter the transport properties of gold nanocontacts. Since this is true for the range of electrode potentials at which the 44bpy molecule binds to the metal,[19] the same minor influence of the solution environment in 44bpy/gold MNBs is also considered. This is also justified by the fact (that will become apparent below) that the nitrogen lone pairs of the molecule are involved in molecule−metal binding, instead of being used in molecule−solvent or molecule−ion interactions. As a side effect, the remaining and most hydrophobic part will maintain a weak interaction with the surrounding water molecules and ions,

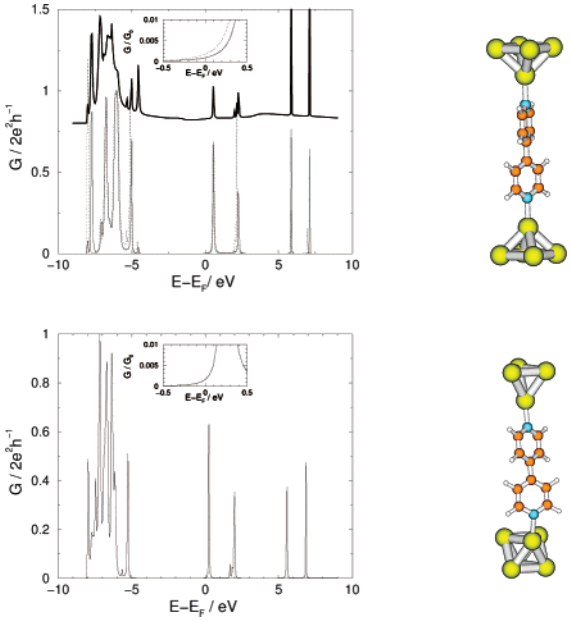

Figure 3. Conductance profiles for two possible 4,4′-bipyridine/gold nanobridges (shown at the right) coming from (001) 4-1-1-4 (upper panel) and (111) 3-1-3-3 (bottom panel) ruptures of the gold nanocontact. The insets represent in more detail the conductance around the Fermi level. The curve in bold face in the upper panel corresponds to the scaled DOS of this MNB, which has also been translated vertically for clarity. The dotted curve in the same panel plots the conductance at the geometry optimized with the LANL2DZ basis set and pseudopotential.

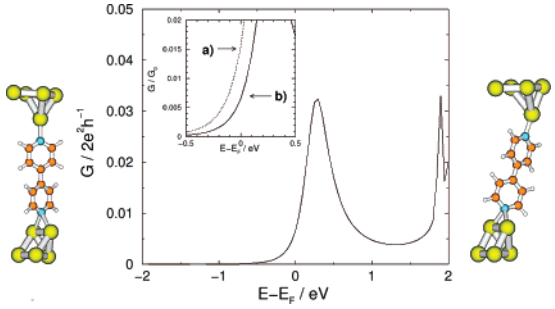

Figure 4. Conductance profiles for two possible 4,4′-bipyridine/gold nanobridges coming from a (111) 3-2-1-4 rupture of the gold nanocontact. The geometry at the right (left) corresponds to a rupture allowing (restricting) the lateral movement of the gold tip. The inset helps to appreciate minor differences in conductance around $0.01G_0$ at the Fermi level between the right and left structures, termed b and a, respectively.

suggesting that the latter will have little influence on the geometry that the 44bpy/gold arrangement adopts.

4.1. Chemical−Transport Interplay in 44bpy/Gold MNBs. As means to find out the geometries of this type of MNB, geometry optimizations have been performed on clusters representing the system. To compare the stationary energies of the different structures and to lower the computational cost of the calculations, the total number of gold atoms representing the leads has been reduced to 10. Extensive use has been made of the ability of Gaussian03 to perform partial optimizations by freezing some variables.[35] Thanks to this, just those degrees of freedom that are relevant for the problem at hand, namely, the 44bpy dihedral angle, the orientation and distance of the 44bpy molecule with respect to the metal tips, and the tip−tip distance are able to be optimized. The rest of the 44bpy internal degrees of freedom are not included in the optimizations, as mentioned in section 2. The interested reader may find additional details on the optimizations in the Supporting Information.

The resulting optimized geometries, termed (001) 4-1-1-4, (111) 3-1-3-3, and (111) 3-2-1-4, have been depicted in Figures 3 and 4. These gold−molecule arrangements represent binding situations between 44bpy and the (001) 9-4-1-1-4-9, (111) 6-3-1-3-6, and (111) 9−5-2-1-3-6 gold nanocontacts introduced above, respectively. The corresponding conductance profiles obtained from these structures after applying the GECM method have also been plotted in these figures. Results representing the (111) 6-3-1-1-3-6 geometry have not been shown since they yield almost the same conductance profiles as those representing the (001) 9-4-1-1-4-9 geometry. To test the reliability of the basis set and pseudopotential used, the geometry optimization of the (001) 4-1-1-4 arrangement with the B3LYP exchange-correlation functional has been repeated but using the larger (and computationally more demanding) LANL2DZ basis set and pseudopotential. Both computations lead to almost the same atomic arrangement, with similar N−Au distances (2.2 vs 2.3 Å for the B3LYP/LANL2DZ and the present model chemistry, respectively) although with a slight difference in dihedral angle (37° vs 32° for B3LYP/LANL2DZ and the present model chemistry, respectively). However, these small changes have a negligible effect on the conductance profile around E_F, as can be seen in the upper panel of Figure 3, where $G(E)$ evaluated with GECM and the present model chemistry is plotted at both the B3LYP/LANL2DZ optimized geometry and at that found with the model chemistry used throughout this work.

From Figures 3 and 4, it can be concluded that (i) the MNB forms through nitrogen−gold interaction and (ii) steric repulsions limit the way the molecule binds to the leads. Of course, point i above is the driving force behind the formation of the MNB; the presence of the nitrogen atoms at each side of the molecule permits establishing the connection between the gold contacts. However, in this case, the steric repulsions caused by the hydrogen atoms *restrict the number of possible molecule−metal arrangements*. Actually, as can be seen in Figures 3 and 4, the 44bpy molecule tries to combine its appetence to form nitrogen−gold bonds *and* to keep as low as possible the aforementioned hydrogen-promoted steric repulsions. The molecule meets this last requirement by placing one of its rings almost perpendicular to the gold−gold bridge in the (111) 3-2-1-4 structure or by keeping a 60° angle between this ring and the gold−gold bridges of the hollow site in the (111) 3-1-3-3 geometry. These two structures are, indeed, less stable than that corresponding to the (001) 4-1-1-4 one, where gold−hydrogen steric repulsions are less important. The energy ordering relative to the (001) 4-1-1-4 structure is +6.1 and +10.5 kcal/mol for the (111) 3-2-1-4 structures in Figures 4b and 4a, respectively and +29.0 kcal/mol for the (111) 3-1-3-3 structure depicted in the bottom panel of Figure 3. However, the N−Au distance in all cases remains at a stable value of about 2.3 Å, with the 44bpy dihedral angle being around 30°, in good agreement with experimental data for the isolated molecule.[45] Thus, the steric repulsions limit the way the molecule orients with respect to the metal tips. This is a first step to explain the *reproducibility* found in the statistical analysis of the conductance done by Xu and Tao.[19] It will be seen below that the nitrogen−gold interaction, besides being the driving force behind the formation of this MNB, is also the next step toward the theoretical interpretation of such reproducibility.

At this point, it is convenient to make a short digression on what happens to a closed system, such as an isolated molecule, when it transforms into an open one by coupling to a pair of semi-infinite electrodes. First of all, the discrete molecular levels

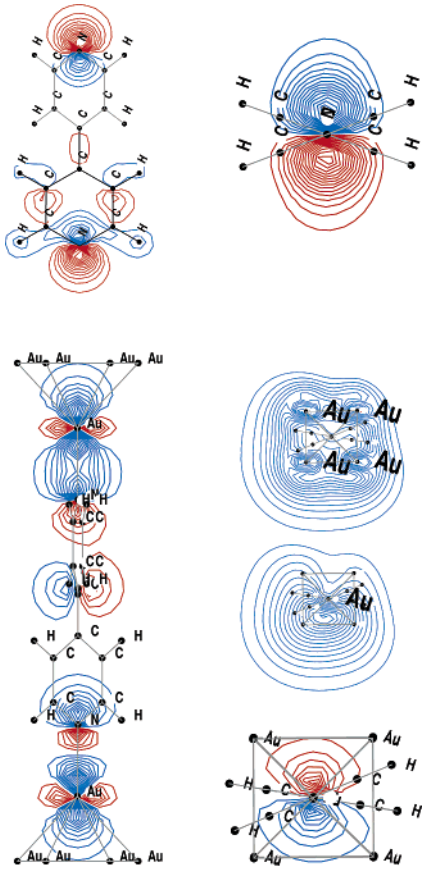

Figure 5. Top left: Contour plot of the HOMO of an isolated bipyridine molecule on a plane including one of the rings. Top right: Same plot for the LUMO on a plane perpendicular to the N−N axis and centered in one of the N atoms. Bottom left: Contour plot of $\rho(\mathbf{r},E)$ (see text) along the tip−tip axis for the HOMO-derived resonance in the (001) 4-1-1-4 MNB. Bottom right: Same for the LUMO-derived resonance at three different planes perpendicular to the tip−tip axis and centered at the four-atom gold plane (top), the on-top gold atom (middle), and the nitrogen atom (bottom).

broaden into a quasi-continuum density of states (DOS) due to hybridization with the metal wave functions. Nevertheless, the DOS often retains a "peaked" structure where the molecular energy levels can be regarded as a group of broadened resonances. This is what happens in the problem at hand; in fact, the underlying level structure of the 44bpy molecule is clearly appreciated in the upper panel of Figure 3. The two curves plotted in this panel correspond to the DOS and the conductance profile obtained after applying the GECM to the (001) 4-1-1-4 structure depicted at the right. The perfect correspondence between both peaked curves reflects that the conductance along the MNB is high whenever the linkage between the molecular orbitals and the metal functions is good. Indeed, the highest occupied molecular orbital (HOMO)−LUMO gap obtained from a DFT calculation on the isolated 44bpy molecule is 4.8 eV, which coincides quite well with the amplitude of the gap in the calculated conductance profile. According to this, the resonances at each side of the gap in Figure 3 can be associated with HOMO- and LUMO-derived bipyridine levels. Further support to this interpretation is given by the contour plots depicted in Figure 5, which furthermore indicate which orbitals are involved in metal−molecule bonding and electronic transport. The two plots at the top of this figure correspond to the HOMO (left) and LUMO (right) orbitals after a DFT geometry optimization of the dihedral angle of an isolated 44bpy molecule has been performed with the same model chemistry used throughout this work. It is evident that the HOMO is dominated by lone-pair sp^2 orbitals, while the LUMO is mainly composed of p_π orbitals. However, the plots at the bottom of Figure 5 represent the so-called spatially resolved density of states $\rho(\mathbf{r},E)$, of the molecule−metal bridge, defined as

$$\rho(\mathbf{r},E) = \sum_m \phi_m(\mathbf{r}) P_m(E) \tag{5}$$

where $\phi_m(\mathbf{r})$ is the mth atomic orbital and $P_m(E)$ is the so-called projected density of states on this orbital, which measures the contribution of orbital ϕ_m to the conducting channels, and is given by

$$P_m(E) = -\frac{1}{\pi} \lim_{\delta \to 0} \mathrm{Im}\, \mathbf{G}^r_{mm}(E) \tag{6}$$

where Im denotes the imaginary part of the corresponding matrix element. Therefore, $\rho(\mathbf{r},E)$ reflects the shape of the channels transmitting at a certain energy. The left (right) plot at the bottom of Figure 5 shows $\rho(\mathbf{r},E)$ of the lower (upper) resonance of the conductance gap shown in Figure 3a. The resemblance with the molecular HOMO and LUMO of the isolated molecule is evident and shows that the resonances at each side of the gap form by hybridization of the HOMO and LUMO of the 44bpy molecule with the Au s and d_0 orbitals in the leads.

In summary of the above discussion, the conductance peak slightly above the Fermi level, which is responsible for the conductance of this nanobridge, is a 44bpy LUMO-derived resonance. The third and last step that closes the theoretical explanation of the conductance in this type of MNB is the positioning of the aforementioned resonance with respect to the Fermi level. In turn, this depends on the amount of charge transferred from the gold atoms to the molecule to achieve a common electrochemical potential throughout the entire system (molecule + electrodes). This charge transfer is lower for the two structures of Figure 3 than that of Figure 4, thus placing the Fermi level inside the gap for the former, which yields values for $\mathbf{G}(E_F)$ at least 1 order of magnitude below the experimental one. Therefore, the (111) 3-2-1-4 structure is left as the only one leading to a conductance at the Fermi energy compatible with the experimental value of $0.01G_0$ proposed in ref 19 for a single bipyridine molecule. It has also been checked that including the lateral displacement of one gold tip with respect to the other in the geometry optimizations of the (111) 3-2-1-4 structure leads also to $\mathbf{G}(E_F) \approx 0.01G_0$, as Figure 4 shows. This stability, together with the fact that it was also a (111) -2-1- type of geometry that best reproduced the conductance quantum of the gold nanocontact, brings consistency to the overall picture. As has been seen, the same arrangement of gold atoms explains both the last conductance plateau of the gold nanocontact breakage and the conductance of the MNB formed upon this rupture, when the 44bpy molecule bridges the gap between the two metallic tips formed.

4.2. Dynamic Behavior of Conducting 44bpy/Gold MNBs. In ref 19, Xu and Tao reported that the conductance plateaus related with the 44bpy molecule, observed in conductance vs STM displacement experiments, are quite long (9 ± 2 Å), on the order of the size of bipyridine (~7 Å). In this section, this finding will attempt to be reconciled with a description of the events occurring at the atomic level. Again, geometry optimizations are performed analogous to those in the previous section prior to the conductance calculations. However, different from such optimizations, all of the coordinates of the gold atoms at

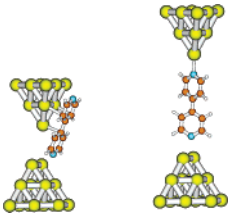

Figure 6. Optimized geometries for a 4,4′-bipyridine molecule bridging two gold tips just after breaking the gold−gold bond (left) and at a much larger tip−tip separation (right).

several tip−tip distance values are now fixed to analyze the dynamic behavior of the conducting MNB. However, the structure found in the previous section whose conductance compared favorably with the experimental one are only focused on, although more gold atoms are included to obtain a more reliable description.

The first and last stages in the process of pulling the STM tip during the formation of the nanobridge can be found in Figure 6. The two structures depicted in this figure correspond to the optimized geometries that have been obtained and that represent, respectively, the situation just after the breaking of the gold nanocontact (left) and after the pulling process has brought the tip and substrate quite far apart from each other (right). The tip−tip distance changes about 7 Å between both geometries. As can be seen, the 44bpy molecule is *already there*, adsorbed on the gold substrate, when the breaking of the gold nanocontact is taking place. However, once the gold−gold distance is sufficiently large, the molecule prefers to bind to the single on-top atom in one of the tips to alleviate the hydrogen−gold steric repulsions.

In regards to the intermediate situations between these two extreme points, Figure 7 shows the optimized geometries adopted by the bipyridine molecule at several tip−tip distances in the pulling process. The tip−tip distances are 7.1, 9.4, and 11.0 Å when going from the structure depicted in Figure 7a to that in Figure 7b to that in Figure 7c. As can be seen, the corresponding value of the conductance at the Fermi level is well-established around $0.03G_0-0.04G_0$, which compares well with the experimental value of $0.01G_0$ assigned to a *single* molecule by Xu and Tao. Therefore, the long conductance plateaus observed in ref 19 can then be attributed to the fact that the bipyridine molecule takes *control* of the conducting process *right after* the breaking of the metal nanocontact through a LUMO-derived resonance. The expected large variability of connecting possibilities as the STM tip is being pulled does not take place since N−Au binding is handicapped by steric repulsions. As can be seen, one nitrogen atom binds to a "bridge" of two gold atoms at one side of the breaking junction, while the other attaches to low-coordination gold atoms placed at one of the edges of the pyramid representing the other part of the former gold nanocontact. The similar bonding scheme effectively maintains the conductance at a stable value controlled by the LUMO-derived resonance. The change observed in the value of $\mathbf{G}(E_F)$ with respect to that obtained in the previous section is due to the increase in the number of metal atoms entering the cluster. Previous work using GECM has shown that these kind of changes quickly achieve convergence after two or three metallic planes have been included in the cluster.[29,31] Therefore, confidence is still retained in the conclusions achieved because the change in $\mathbf{G}(E_F)$ is not large and because the rest of the structures yield values 1 order of magnitude below the experimental one. It is also important to stress that it is not the I/V characteristics or the conductance at

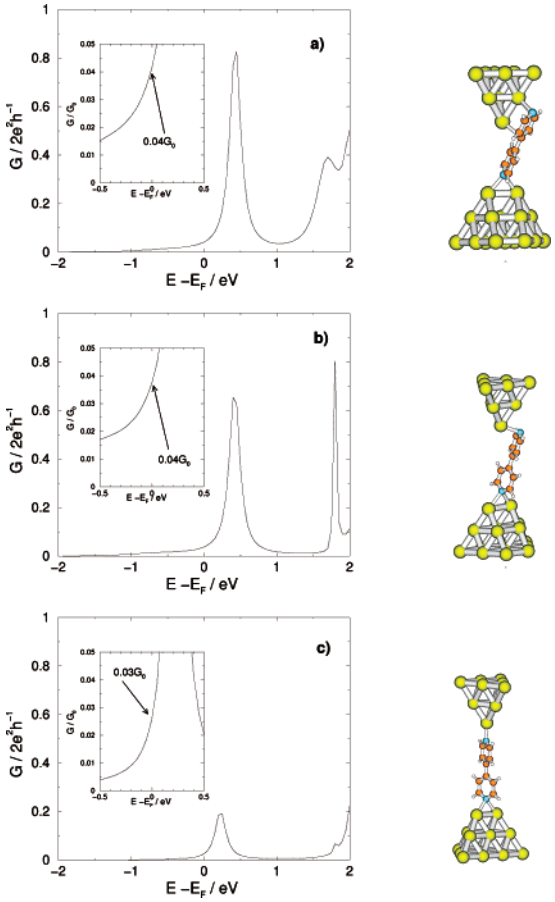

Figure 7. Conductance profiles for the 4,4′-bipyridine gold attachments shown at the right, as the gold tips are being pulled apart. The insets represent in more detail the conductance around the Fermi level.

zero bias that is of primary importance in this molecular nanobridge (indeed, the latter is rather small compared to that obtained with other molecular bridges) but rather its remarkable reproducibility. In this sense, the computations performed in this work have been able to *explain* such reproducibility.

Recall also that three 44bpy molecules could attach to this metallic arrangement with a similar binding scheme; each would have one nitrogen bridging two gold atoms at one side of the gold contact (that with the trapezoidal form) while the other nitrogen is bonded to one of the *three* edges of the other gold tip. It is clear that, upon pulling the leads apart, the two "side" molecules would eventually fail to "bridge de gap" before that same thing happens to the "central" one, thus explaining the sequence of conductance plateaus of $0.03G_0$, $0.02G_0$, and $0.01G_0$ that sometimes are found in ref 19. Unfortunately, the computational effort to perform a geometry optimization for such a large system prevents giving stronger support to this explanation, leaving this topic as an open question.

5. Conclusions

The analysis performed in the previous sections has helped to establish the connection between the physicochemical and conductance properties of 4,4′-bipyridine/gold MNBs. This interconnection can be summarized in the following issues:

(i) The driving force for the formation and stability of these type of MNBs is the hybridization between the HOMO and LUMO of 44bpy with the s and d orbitals from low-coordination gold atoms in the leads.

(ii) The molecule orientation with respect to the gold structure is restricted due to hydrogen-promoted steric repulsions, thus

preventing the formation of a large number of molecule−metal arrangements.

(iii) The positioning of the Fermi level near a LUMO-derived resonance by means of charge transfer from the metal to the molecule eliminates reasonable structures from the set of conducting representatives for this MNB by placing E_F inside the "molecular" HOMO−LUMO gap.

(iv) Only one structure provides a conductance at the Fermi energy compatible with the experimental results, which explains the reproducibility of the latter. The gold arrangement of this structure provides also a good description of the last stage in the breaking process of the gold nanocontact. This structure should be considered as part of a family of similar atomic arrangements contributing most to the conductance peak in the experimental histograms.

(v) As the STM tip is being pulled away from the sample, the 4,4′-bipyridine molecule "adapts" to the evolving environment according to the above-mentioned electron-binding and steric-repulsion phenomena without appreciable changes in $\mathbf{G}(E_F)$, in accordance with the long size of the experimental conductance plateaus.

(vi) The structure proposed to explain the conductance observed for 44bpy/gold MNBs is consistent with at most three bipyridine molecules bonded in a similar fashion and thus providing the same conductance. They nevertheless have foreseeable differences in regards to the distance at which they can bridge the gap between the gold tips, which could explain the steps seen in some of the experimental conductance traces.

The conclusions summarized above should help scientists when selecting candidate molecules to build efficient and reproducible MNBs, by taking into account not only their electronic properties to form stable molecular junctions but also their structural characteristics to reduce the number of possible conducting structures.

Acknowledgment. Financial support from the Spanish MCYT through projects BQU2001-0883, PB96-0085, and MAT2002-04429-C03 is gratefully acknowledged. The author thanks the Spanish MCYT for a research contract under the "Ramón y Cajal" program and the Generalitat Valenciana and the Universidad de Alicante for economic support. Fruitful discussions with Professor J. J. Palacios are also kindly acknowledged.

Supporting Information Available: Further details on the geometry optimizations and Cartesian coordinates for all of the optimized structures. This material is available free of charge via the Internet at http://pubs.acs.org.

References and Notes

(1) Pascual, J. I.; Méndez, J.; Gómez-Herrero, J.; Baró, A. M.; García, N. *Phys. Rev. Lett.* **1993**, *71*, 1852−1855.

(2) Pascual, J. I.; Méndez, J.; Gómez-Herrero, J.; Baró, A. M.; García, N.; Landman, U.; Luedtke, W. D.; Bogacheck, E. N.; Cheng, H.-P. *Science* **1995**, *267*, 1793−1795.

(3) Ohnishi, H.; Kondo, Y.; Takanayagi, K. *Nature* **1998**, *395*, 780−783.

(4) Rubio-Bollinger, G.; Bahn, S. R.; Agraït, N.; Jacobsen, K. W.; Vieira, N. *Phys. Rev. Lett.* **2001**, *87*, 026101.

(5) Takai, Y.; Kawasaki, T.; Kimura, Y.; Ikuta, T.; Shimizu, R. *Phys. Rev. Lett.* **2001**, *87*, 106105.

(6) Yanson, A. I.; Rubio-Bollinger, G.; van der Brom, H. E.; Agraït, N.; van Ruitenbeek, J. M. *Nature* **1998**, *395*, 783−785.

(7) Agraït, N.; Levy Yeyati, A.; van Ruitenbeek, J. M. *Phys. Rep.* **2003**, *377*, 81−279.

(8) Bockrath, M.; Cobden, D. H.; McEuen, P. L.; Chopra, N. G.; Zettl, A.; Thess, A.; Smalley, R. E. *Science* **1997**, *275*, 1922−1925.

(9) Reed, M. A.; Zhou, C.; Mullen, C. J.; Burgin, T. P.; Tour, J. M. *Science* **1997**, *278*, 252−254.

(10) Fink, H.-W.; Schönenberger, C. *Nature* **1999**, *398*, 407−410.

(11) Porath, D.; Bezryadin, A.; de Vries, S.; Dekker, C. *Nature* **2000**, *403*, 635−638.

(12) Liang, W.; Shores, M. P.; Bockrath, M.; Long, J. R.; Park, H. *Nature* **2002**, *417*, 725−729.

(13) Mayor, M.; von Hänisch, C.; Weber, H. B.; Reichert, J.; Beckmann, D. *Angew. Chem., Int. Ed.* **2002**, *41*, 1183−1186.

(14) Park, J.; Pasupathy, A.; Goldsmith, J. I.; Chang, C.; Yaish, Y.; Petta, J. R.; Rinkoski, M.; Sethna, J. P.; Abruña, H.; McEuen, P. L.; Ralph, D. C. *Nature* **2002**, *417*, 722−725.

(15) Smit, R. H. M.; Noat, Y.; Untiedt, C.; Lang, N. D.; van Hemert, M. C.; van Ruitenbeek, J. M. *Nature* **2002**, *419*, 906−909.

(16) García, Y.; Palacios, J. J.; SanFabián, E.; Vergés, J. A.; Pérez-Jiménez, A. J.; Louis, E. *Phys. Rev. B* **2004**, *69*, 041402(R).

(17) Shu, C.; Li, C. Z.; He, H. X.; Bogozi, A.; Bunch, J. S.; Tao, N. J. *Phys. Rev. Lett.* **2000**, *84*, 5196−5199.

(18) Xu, B.; He, H.; Tao, N. J. *J. Am. Chem. Soc.* **2002**, *124*, 13568−13575.

(19) Xu, B.; Tao, N. J. *Science* **2003**, *301*, 1221−1223.

(20) Datta, S. *Electronic Transport in Mesoscopic Systems*; Cambridge University Press: Cambridge, 1995.

(21) Mujica, V.; Kemp, M.; Ratner, M. A. *J. Chem. Phys.* **1994**, *101*, 6849−6855.

(22) Hirose, K.; Tsukada, M. *Phys. Rev. B* **1995**, *51*, 5278−5290.

(23) Lang, N. D. *Phys. Rev. B* **1995**, *52*, 5335−5342.

(24) Emberly, E. G.; Kirczenow, G. *Phys. Rev. B* **1998**, *58*, 10911−10920.

(25) Yaliraki, S.; Roitberg, A. E.; Gonzalez, C.; Mujica, V.; Ratner, M. A. *J. Chem. Phys.* **1999**, *111*, 6997−7002.

(26) Derosa, P. A.; Seminario, J. M. *J. Phys. Chem.* **2001**, *105*, 471−481.

(27) Taylor, J.; Guo, H.; Wang, J. *Phys. Rev. B* **2001**, *64*, 245407.

(28) Di Ventra, M.; Kim, S.-G.; Pantelides, S. T.; Lang, N. D. *Phys. Rev. Lett.* **2001**, *86*, 288.

(29) Palacios, J. J.; Pérez-Jiménez, A. J.; Louis, E.; Vergés, J. A. *Phys. Rev. B* **2001**, *64*, 115411.

(30) Brandbyge, M.; Taylor, J.; Stokbro, M.; Mozos, J. L.; Ordejón, P. *Phys. Rev. B* **2002**, *65*, 165401.

(31) Palacios, J. J.; Pérez-Jiménez, A. J.; Louis, E.; SanFabián, E.; Vergés, J. A. *Phys. Rev. B* **2002**, *66*, 035322.

(32) Louis, E.; Vergés, J. A.; Palacios, J. J.; Pérez-Jiménez, A. J.; SanFabián, E. *Phys. Rev. B* **2003**, *67*, 155321.

(33) Pérez-Jiménez, A. J.; Palacios, J. J.; Louis, E.; SanFabián, E.; Vergés, J. A. *ChemPhysChem* **2003**, *4*, 388−392.

(34) Palacios, J. J.; Pérez-Jiménez, A. J.; Louis, E.; SanFabián, E.; Vergés, J. A. *Phys. Rev. Lett.* **2003**, *90*, 106801.

(35) Frisch, M. J.; Trucks, G. W.; Schlegel, H. B.; Scuseria, G. E.; Robb, M. A.; Cheeseman, J. R.; Montgomery, Jr., J. A.; Vreven, T.; Kudin, K. N.; Burant, J. C.; Millam, J. M.; Iyengar, S. S.; Tomasi, J.; Barone, V.; Mennucci, B.; Cossi, M.; Scalmani, G.; Rega, N.; Petersson, G. A.; Nakatsuji, H.; Hada, M.; Ehara, M.; Toyota, K.; Fukuda, R.; Hasegawa, J.; Ishida, M.; Nakajima, T.; Honda, Y.; Kitao, O.; Nakai, H.; Klene, M.; Li, X.; Knox, J. E.; Hratchian, H. P.; Cross, J. B.; Bakken, V.; Adamo, C.; Jaramillo, J.; Gomperts, R.; Stratmann, R. E.; Yazyev, O.; Austin, A. J.; Cammi, R.; Pomelli, C.; Ochterski, J. W.; Ayala, P. Y.; Morokuma, K.; Voth, G. A.; Salvador, P.; Dannenberg, J. J.; Zakrzewski, V. G.; Dapprich, S.; Daniels, A. D.; Strain, M. C.; Farkas, O.; Malick, D. K.; Rabuck, A. D.; Raghavachari, K.; Foresman, J. B.; Ortiz, J. V.; Cui, Q.; Baboul, A. G.; Clifford, S.; Cioslowski, J.; Stefanov, B. B.; Liu, G.; Liashenko, A.; Piskorz, P.; Komaromi, I.; Martin, R. L.; Fox, D. J.; Keith, T.; Al-Laham, M. A.; Peng, C. Y.; Nanayakkara, A.; Challacombe, M.; Gill, P. M. W.; Johnson, B.; Chen, W.; Wong, M. W.; Gonzalez, C.; Pople, J. A. *Gaussian 03*, revision B.01; Gaussian, Inc.: Wallingford, CT, 2004.

(36) Becke, A. D. *J. Chem. Phys.* **1993**, *98*, 5648−5652.

(37) Stephens, P. J.; Devlin, F. J.; Chablowski, C. F.; Frisch, M. J. *J. Phys. Chem.* **1994**, *98*, 11623−11627.

(38) Pacios, L. F.; Christiansen, P. A. *J. Chem. Phys.* **1985**, *82*, 2664−2671.

(39) Roos, R. B.; Powers, J. M.; Atashroo, T.; Ermler, W. C.; LaJohn, L. A.; Christiansen, P. A. *J. Chem. Phys.* **1990**, *93*, 6654−6670.

(40) Dunning, T. H., Jr. *J. Chem. Phys.* **1989**, *90*, 1007−1023.

(41) Dunning, T. H., Jr.; Hay, P. Gaussian Basis Sets for Molecular Calculations. In *Methods of Electronic Structure Theory*; Schaefer, H. F., III, Ed.; Plenum: New York, 1977.

(42) Hay, P. J.; Wadt, W. R. *J. Chem. Phys.* **1985**, *82*, 270−283.

(43) Wadt, W. R.; Hay, P. J. *J. Chem. Phys.* **1985**, *82*, 284−298.

(44) Hay, P. J.; Wadt, W. R. *J. Chem. Phys.* **1985**, *82*, 299−310.

(45) *CRC Handbook of Chemistry and Physics*, 84th ed.; Lide, D. R., Ed.; CRC Press LLC: New York, 2003.

(46) Kondo, Y.; Takayanagi, K. *Phys. Rev. Lett.* **1997**, *79*, 3455−3458.
(47) Kizuka, T. *Phys. Rev. Lett.* **1998**, *81*, 4448−4451.
(48) Rodrigues, V.; Ugarte, D. *Phys. Rev. B* **2001**, *63*, 073405.
(49) Rego, L. G. C.; Rocha, A. R.; Rodrigues, V.; Ugarte, D. *Phys. Rev. B* **2003**, *67*, 045412.
(50) Rodrigues, V.; Fuhrer, T.; Ugarte, D. *Phys. Rev. Lett.* **2000**, *85*, 4124.
(51) Häkkinen, H.; Barnett, R. N.; Scherbakov, A. G.; Landman, U. *J. Phys. B* **2000**, *104*, 9063−9066.
(52) da Silva, E. Z.; da Silva, A. J. R.; Fazzio, A. *Phys. Rev. Lett.* **2001**, *87*, 256102.
(53) da Silva, E. Z.; Novaes, F. D.; da Silva, A. J. R.; Fazzio, A. *Phys. Rev. B* **2004**, *69*, 115411.
(54) Zhuang, M.; Ernzerhof, M. *J. Chem. Phys.* **2004**, *120*, 4921−4926.